Toward a Patient-specific Image Data-driven Predictive Modeling Framework for Guiding Microwave Ablative Therapy

Michael I. Miga[1], Jarrod A. Collins[1], Jon S. Heiselman[1], and Daniel B. Brown[2]

[1] Vanderbilt University, Nashville, TN 37235, USA
[2] Vanderbilt University Medical Center, Nashville, TN 37232, USA
Michael.Miga@vanderbilt.edu

Abstract. In this work, a preliminary effort toward a novel multi-physics modeling framework is presented that combines computational approaches in soft-tissue biomechanics, and bioelectric/bioheat transport to create a patient-specific, image-data driven guidance platform to improve localization and predict thermal dose extent for microwave ablation. More specifically, a finite element modeling and optimization approach for microwave ablation delivery is driven by sparse intra-procedural geometric digitization, and pre-procedural imaging data for providing image-to-physical registration, and dielectric property estimates, respectively. In a series of mock liver phantom experiments, the framework is explored herein. Results indicate superior localization using our non-rigid registration approach, and accurate prediction of lesion formation using our image-data-driven approach to ablation forecasting. Results also provide insight on the impact of localization and material property inaccuracies with respect to therapy delivery and show systematic and considerable degradation of lesion-to-target overlap.

Keywords: Image Guidance, Microwave Ablation, Finite Element, Registration, Modeling, Deformation.

1 Introduction

1.1 Clinical Background

Hepatic tumors are a major U.S. and worldwide health care concern with the rate of primary liver cancer (HCC) continuing to rise [1]. Along with hepatocellular carcinoma, many primary neoplasms also metastasize to the liver. With respect to treatment, resection and transplant are the best options but eligibility, and scarcity still limit candidacy, respectively. For example, based on one study involving 2400 subjects, only 20% of patients were eligible for surgical resection due to risk [2]. When faced with these challenges or extensive multi-focal disease, procedures become multimodal and dynamic, e.g. physicians are exploring with staging and then among those stages combining approaches to include resection, loco-regional ablative, arterial, and conventional systemic therapies (e.g. resection combined with ablation, two-stage resection,

ablation, radio/chemo-embolic procedures, etc.). This represents a movement toward a more chronic management viewpoint of disease with goals of facilitating surgery, bridge-to-transplant, and/or extending quality of life. Microwave ablation (MWA) is certainly one of the more promising thermal ablative technologies for the locoregional control of liver cancer [3-6]. Some studies suggest a 5-year survival rate with MWA that is comparable to surgical resection [7]. Nevertheless, with ~80% of patients ineligible for resection/transplant [8], increasing MWA efficacy is certainly warranted.

1.2 Scientific Premise

Building on the promise of MWA, the underpinning premise of the work reported here is that improving MWA therapy is intrinsically dependent on the ***precise localization*** and ***determination of dose extent*** in relation to spatially-encoded disease information, i.e. anatomically-annotated, disease-related biomarkers usually provided by imaging. Without the ability to accurately localize: analysis of outcomes for determining procedural efficacy, understanding the morphology of recurrence, comparing therapeutic approaches, evaluating technique improvements, and investigating the impact of imaging biomarkers to drive therapy decisions will remain ambiguous.

With respect to ***localization*** specifically, in a recent n=176 patient study looking at long-term outcomes of MWA for liver malignancies, the investigators reported a 17.6% local recurrence rate with rates increasing with tumor size, i.e. recurrence rates spanning from 1%-33% for tumors sizes ranging from <1cm to >3cm, respectively [9]. Clearly, outcomes are compromised with size but does the cause reside with the ability to localize delivery? or with the imaging information driving the ablation? or with soft-tissue characteristics affecting plans (e.g. material properties, deformation, etc.)? or perhaps it resides in our understanding of tumor phenotype in large lesions? The cause is likely a combination of factors. Unfortunately however, studies specifically looking at the causes of recurrence are sparse and difficult to achieve in light of a lack of precision in localization. Addressing this need is certainly a fundamental component for treatment quantification to better understand recurrence in human systems.

With respect to the ***determination of dose extent***, strategies in thermography are actively under investigation within the MR (e.g. [10]) and US (e.g. [11]) communities. As a general statement, these sources of data are powerful but in the practical surgical/interventional suite are typically incomplete, cumbersome, and with varying degrees of reproducibility. Also, thermal ablation is a temporally and spatially evolving event. While thermal distributions could inform, they do not necessarily predict/protect against excessive damage to healthy liver, biliary ducts, or nearby organs. In addition, it is also important to recognize that with a dose plan based on a preoperative organ configuration, to what degree intraoperative soft tissue changes affect that delivery dose plan is unknown. From the literature, it is clear that evolving cumulative thermal dose during a hyperthermic ablative procedure is an important factor in determining tissue damage and coverage [12]. Accurate predictive dosing frameworks would allow for better control of the temporal and spatial evolution of MWA-induced thermal energy.

From that arises another question, how does one 'tune' a thermal dose to a particular patient? Efforts toward this are quite sparse. It is generally accepted that variability in dielectric and thermal properties persist in healthy and diseased tissue (e.g. fatty liver, fibrosis, and malignant tissue) and are affected by temperature as well. Methods designed to address these questions in the determination of MWA dose extent are a real clinical need.

2 Methods

In this paper, a multi-physics modeling approach has been adopted to address the uncertainty in the delivery of MWA. More specifically, a biomechanical model is used to non-rigidly correct for deformations occurring intra-procedurally, and a bioelectric/bioheat transport model is used to estimate microwave thermal dose extent. When coupled together, these create a comprehensive framework to accurately forecast therapeutic delivery and extent. In the below sections, we briefly describe our approach and our experimental evaluation.

2.1 Correcting for Intra-procedural Deformations

The methods employed in this work are specifically designed to using computational biophysical models for image-to-physical non-rigid liver registration using sparse data compatible with open surgery and interventional presentations [13, 14]. The methodology is an inverse boundary condition reconstruction approach designed to match shape change as defined between preoperative and intraoperative organ states. Briefly, the methodology begins with the spatial designation of liver salient features (usually these are associated with ligament attachments and/or liver ridges) on both the subject's images and the intraoperative physical space counterpart. In the open surgery environment, the physical data can be provided by a tracked stylus being used to swab the organ surface (or with a laser scanner, stereo-camera, etc.). In the interventional environment, often the entire surface of the liver can be extracted from a computed tomography scan. In either case, the physical salient features and their preoperatively imaged counterparts are acquired which is subsequently followed by a more general acquisition of areas of the organ surface that are not salient features. This latter step captures additional intra-procedural shape characteristics. Once geometric data has been acquired, a two-step registration process begins, i.e. a rigid registration using salient features followed by non-rigid fitting process driven by all available sparse data. In the non-rigid registration process, boundary condition nodes from the biomechanical finite element model are associated with *active control surfaces* which will be allowed to drive shape change. In the current realization for open surgery, typically the posterior liver surface is designated as the *active control surface*, and in the context of interventional work, the entire liver surface is employed.

Going further, once the control surfaces are designated on the preoperative liver model, a preoperative computation phase begins where systematic perturbations to the *active*

control surfaces are performed with each perturbation providing a boundary condition set to a highly resolved biomechanical finite element model; and naturally, a series of solutions is produced among the perturbations. These solutions provide an approximation to a Jacobian which is subsequently used within a least-squared sparse data/surface error minimization process. We should note that each iteration has an additional distributed loading filter to create more natural deformations. This completes the preoperative computing phase. With this determination of the Jacobian performed pre-procedurally, real time non-rigid fitting of preoperative liver images to intra-procedural sparse digitization data of the liver can ensue. While investigations are continuing in this approach, the most recently published realization can be found in [15]. It should also be noted that a conventional linear elastic model is employed to reflect the deformation behavior of the liver when subjected to intra-procedural forces. This is represented by the partial differential equation of static mechanical equilibrium, $\nabla \cdot \sigma = 0$, where σ is the mechanical stress tensor. In this description, the constitutive law that relates the mechanical stress to strain is associated with conventional linear theory (i.e. a Hookean solid) [16]. It should be noted that the non-rigid fitting phase involves both rigid and non-rigid components thus capturing some of the global rigid body motion while compensating for deformation.

2.2 Forecasting Intra-procedural Microwave Thermal Dose

The thermal dose to tissue was estimated using COMSOL Multiphysics (COMSOL Inc, Burlington, MA) modeling for simulating electromagnetic wave propagation and heat transfer. The development and absorption of electromagnetic waves radiating from the antenna within the phantom, when assuming no initial existing charge, is described by the electromagnetic wave equation $(\nabla^2 + \omega^2 \mu \varepsilon_c)\vec{E} = 0$ where ω [rad/s] is the angular frequency of the electromagnetic wave, μ [H/m] is the permeability, ε_c is the complex permittivity, and $\vec{E}$ [V/m] is the electric field strength. Heat transfer and the resulting temperature history were solved using Pennes' bioheat equation $\rho c \frac{\partial T}{\partial t} = \nabla \cdot k \nabla T + Q - Q_p + Q_m$ where ρ [kg/m^3] is mass density, c [J/kg·K] is specific heat capacity, k [W/m·K] is thermal conductivity, T [K] is temperature, Q [W/m^3] is heat generation due to absorbed electromagnetic energy, Q_p [W/m^3] is heat loss due to perfusion, and Q_m [W/m^3] is metabolic heat generation. Metabolic heat generation (Q_m) is typically neglected, perfusion (Q_p) is modeled as $m(T - T_h)$ with m as thermal perfusion transfer coefficient, and T_h as homeostatic temperature. Heat generation from power deposition by the applied electric field is calculated by $Q = \frac{1}{2}\sigma \|E\|^2$ where σ [S/m] is the electrical conductivity. The antenna is modeled as a conventional conductive core surrounded by dielectric material, surrounding catheter, with ring shaped slot cut on the outer conductor. Conductive material is not specifically realized but represented by the boundary condition, $\vec{n} \times \vec{E} = 0$. The microwave source itself is modeled as a port boundary condition which relates the field to the square root of the time average power flow in the cable and is adopted from [17]. Boundary conditions reflect a first order electromagnetic scattering condition applied to the exterior of the phantom to eliminate

reflection of outgoing waves by simulating a transparent boundary. Far-field boundaries on exterior are set to homeostatic/outside-environment temperatures. Saline cooling of the antenna was simulated as a convective heat flux condition along the inner boundary of the antenna. Thermally-induced tissue damage is a function of both instantaneous temperature and thermal history. For this work, a modified Arrhenius damage integral is used to estimate the complete ablative zone (in the phantom work, protein denaturation is used as a proxy). The tissue integral takes the form of $\alpha = \int_0^t Aexp\left(-\frac{E_a}{RT(t)}\right)dt$ where α is the degree of damage at a given time, A [1/s] is the frequency factor, E_a [J/mol] is the activation energy required to damage the mock tissue, R [J/mol·K] is the universal gas constant, and $T(t)$ [K] is the temperature history of the tissue/mock-tissue. The fraction of damaged tissue was then determined by $\theta_d = 1 - e^{-\alpha}$. The current framework uses a 2-D axisymmetric model for simplicity. Additional detail can be found in [18].

2.3 Experimental Procedure

With respect to the experimental framework, a custom deformable ablation phantom in the shape of a patient liver (a heat-sensitive gel phantom consisting of liquid egg whites, and agar gel) was created and deformations similar to those experienced between diagnostic, and intra-procedural presentation were applied. With phantoms constructed, a Perseon ST (Perseon Medical, Salt Lake City, UT) microwave antenna was used to generate three separate ablations in each mock human liver and a hi-resolution MR image volume was obtained. After the application of deformation, a repeat MR was performed. This procedure was performed in n=3 phantoms with 4 different deformation states. From this data set, mock liver surfaces were extracted and used with our image-to-physical non-rigid registration approach in the context of open surgical (sparse anterior surface), and interventional procedures (full surface). With each phantom and each deformation, a total of 9 targets could be used to quantify localization error (3 antenna tip locations, 3 antenna insertion points, and 3 ablation centroids). True ablation locations could be determined from the repeat MR imaging. It should be noted that in work not reported here, mock gross pathology has been performed to confirm physical ablation sizes are represented accurately by our MR-measured estimates. In addition, optimal dielectric properties matching the ablation predictions to measurement were previously performed using controlled localization experiments over multiple phantoms. While this approach to determining dielectric properties is not amenable to a prospective ablation, i.e. the clinically translated counterpart, this limitation is addressed in the discussion. Finally, given this experimental setup, a comparison study of lesion prediction to ground truth ablation was conducted. In addition, to understand the impact of dielectric properties, forecasted lesions were compared between the optimized properties and those estimated from volume fractions of components based on literature values. The metric used for evaluating this work was the positive predictive value (PPV) calculated by $PPV = \frac{N_{TP}}{(N_{TP}+N_{FP})}$, where N_{TP} is the volume of the model-predicted ablation zone overlapping with the observed ablation zone, and N_{FP} is the

volume of the model-predicted ablation zone which does not overlap with the true ablation zone.

3 Results

With respect to localization, our biomechanically model-driven image-to-physical registration methodology to correct for deformation performed quite well. In the case of partial surface availability for registration, the average target registration error was 6.0 ± 2.3 mm and 3.7 ± 1.4 mm for rigid and non-rigid registration over all phantoms, respectively. When the full surface of the liver could be used, the average target registration error was 5.6 ± 2.3 mm and 2.5 ± 1.1 mm for rigid and non-rigid registration over all phantoms, respectively. Similarly, when comparing the predicted ablation relative to ground truth, the volumetric overlap was 67.0 ± 11.8%, and 85.6 ± 5.0% for rigid and non-rigid registration, respectively. Fig. 1 *upper panel* is an example analysis from our mock phantom experiments that compares the true ablation as documented by imaging (green) with the model-predicted ablation (red) within the context of conventional rigid registration. In Fig. 1 *lower panel*, the analogous comparison is done, except in this case, our novel non-rigid registration has been employed for targeting the predicted ablation location (blue). Fig. 2 is a comprehensive figure that shows the target error and PPV results over all n=3 phantoms with 4 deformations per phantom and 9 targets per phantom. On the x-axis, the figure illuminates the localization error using sparse anterior (open surgery setting) and full surface (interventional setting) surface data and among both conventional rigid and our novel non-rigid registration methodologies. On the y-axis, the PPV for each ablation is reported which provides a sense of predicted-to-measured lesion overlap for all phantoms. In addition, located on the y-

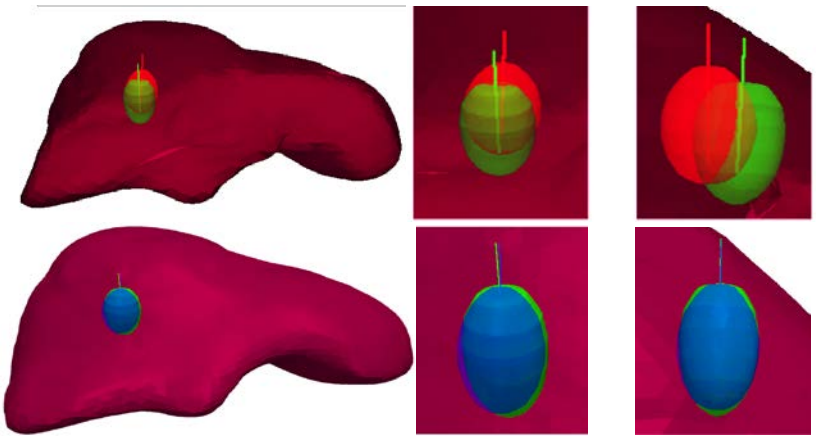

Fig. 1 Ablation model prediction example following registration with full anterior surface data. Green represents ground truth ablation. The rigidly registered ablation model is presented in the top panels (red). The registered ablation model following deformation correction is presented in the lower panels (blue). Additionally, in each panel the registered ablation antenna indicated by lines with color corresponding to the registration method.

axis in red, the maximum possible PPV is provided, i.e. this is a direct model-to-physical ablation comparison with controlled localization in an idealized setup. Fig. 3 shows the results from Fig.2 with respect to optimized properties when the full surface is used for registration. As a comparator, rather than using the optimized dielectric model properties, dielectric properties based on the volume fraction of components and literature values were utilized to compare the PPV under an educated 'guess' environment.

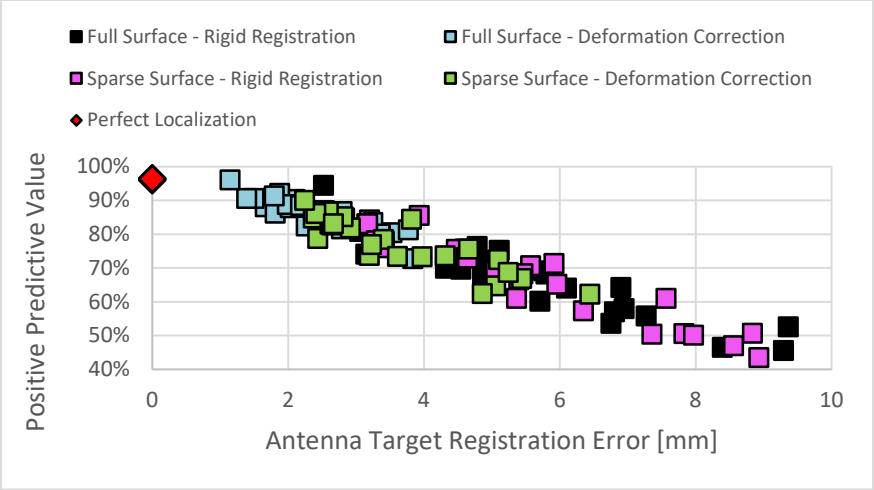

Fig. 2. Positive predictive value is presented for each registered ablation as a function of average target registration of corresponding ablation antenna. MWA model maximum PPV assuming perfect localization is in red.

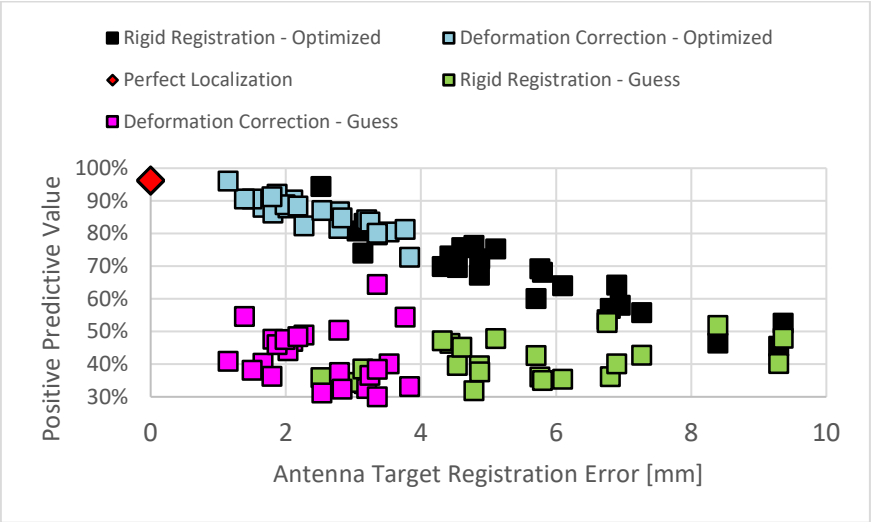

Fig. 3. Positive predictive value is presented for each registered ablation as a function of average target registration of corresponding ablation antenna. Results of the rigid, and non-rigid registration method are presented in black, and blue using image-data-driven calibrated dielectric properties. The counterpart using volume fraction components and literature values used in green, and magenta, respectively. MWA model maximum predictive power assuming perfect registration is in red.

4 Discussion

Overall the results demonstrate that our non-rigid approach to registration reduced localization error. It can also be seen that there is a difference in registration fidelity based on the level of sparsity, which is anticipated. One interesting result is that our non-rigid registration result using only partial surface data outperformed the rigid registration result using the entire surface. Another anticipated result confirmed was that as target error improved, the PPV of our MWA forecasted ablation also improved. The result in Fig. 2 is quite interesting in that it essentially represents a model of PPV degradation as a function of antenna localization error. It suggests, at least in this idealized experiment, that with each 1 mm of antenna localization error, an approximate 5-6% degradation in PPV ensues. While clearly this is an idealized experiment, it does provide some measure of uncertainty in therapeutic delivery which may be an important factor in designing advanced guidance protocols. Fig. 3 is also interesting where it also demonstrates a PPV degradation but in this case as a function of the material properties in our bio-electric/heat transport model of the ablation process. It demonstrates that even in cases of precise localization, it is possible that a mismatch in model dielectric properties could result in an under-prediction of lesion forecasting by a considerable amount.

While the above is interesting, it must be put into context with respect to the limitations of the study. This is a phantom study and while our phantom properties are similar to liver, ultimately, the phantom is not structurally similar. For example, major vasculature and perfusion effects are missing. Another limitation is that this experimental setup was not achieved in a true targeting fashion. More specifically, the ablation was performed on the phantom in three locations and then imaged, and then subsequently it was deformed and re-imaged. This allows the ablation itself to become essentially a therapeutically generated target. The better experiment is to create a real physical target within the phantom itself detectable by imaging, image the phantom to find the target before the procedure, and then plan delivery, then apply deformation, and re-image to determine the organ shape in its deformed state (in addition, it provides true target location within the intraoperative presentation). Once re-imaged, using the navigation system as intended (picking a registration method), navigate to target, ablate, and then compare to ground truth target imaged prior to ablation. This would allow a much better and more therapeutically realistic comparison. Lastly, another limitation is our use of linearized biophysics for our modeling efforts. Conventional thought is that ablation is a nonlinear event and that constitutive properties will be sensitive to thermal changes among others. Considering Fig. 3, changes in properties are quite important. The work presented here is essentially a linearized fit to a nonlinear problem. It remains to be seen if a linearized forecasting approach is sufficient to provide therapeutic benefit when used within a planning system. We should note however that the concept of using image-data-driven approach to estimate dielectric properties is not remote. In work not reported here, we have performed phantom experiments similar to those above using a commercially available fat quantification sequence, mDixon Quant, to acquire images

of phantoms with varying fat content and demonstrated a relationship between fat content and dielectric and thermal material property changes such that a surrogate image-based biomarker could establish appropriate values for the modeling framework in a prospective manner. In those experiments, fat content in the phantom varied between 0-10%, a range quite similar to that found in fatty liver disease, a condition on the rise in presentation and rapidly replacing viral- and alcohol-related liver disease as a major factor in HCC [19]. It is intriguing to consider imaging extending beyond anatomical information to a series of prospective image-based biomarker surrogates that could establish mechanical, electrical, thermal, and perfusion properties of liver tissue to create an accurate MWA forecasting computational environment. This does not necessarily answer the question as to the importance of nonlinear effects; however, the work here does represent first steps in being able to study this behavior.

5 Conclusions

This paper has demonstrated a complex multi-physics modeling approach to estimate MWA dose extent in liver. The approach proposes to use imaging data and biomechanical models as a means to enhance localization of MWA delivery. The approach goes further by using imaging data as a comprehensive step in model initialization of a bioelectric/heat model such that accurate MWA is forecast. While presented here in a mock tissue environment, the quantitative results are quite encouraging.

Acknowledgements: This work was supported by the National Institutes of Health with awards R01CA162477 from the National Cancer Institute and T32EB021937 from the National Institute of Biomedical Imaging and Bioengineering

References

1. American Cancer Society: Cancer Facts and Figures 2018. American Cancer Society (2018)
2. Nikfarjam, M., Shereef, S., Kimchi, E.T., Gusani, N.J., Jiang, Y.X., Avella, D.M., Mahraj, R.P., Staveley-O'Carroll, K.F.: Survival Outcomes of Patients with Colorectal Liver Metastases Following Hepatic Resection or Ablation in the Era of Effective Chemotherapy. Annals of Surgical Oncology 16, 1860-1867 (2009)
3. Tanaka, K., Shimada, H., Nagano, Y., Endo, I., Sekido, H., Togo, S.: Outcome after hepatic resection versus combined resection and microwave ablation for multiple bilobar colorectal metastases to the liver. Surgery 139, 263-273 (2006)
4. Vasnani, R., Ginsburg, M., Ahmed, O., Doshi, T., Hart, J., Te, H., Ha, T.G.V.: Radiofrequency and microwave ablation in combination with transarterial chemoembolization induce equivalent histopathologic coagulation necrosis in hepatocellular carcinoma patients bridged to liver transplantation. Hepatobiliary Surgery and Nutrition 5, 225-233 (2016)
5. Tinguely, P., Fusaglia, M., Freedman, J., Banz, V., Weber, S., Candinas, D., Nilsson, H.: Laparoscopic image-based navigation for microwave ablation of liver tumors-A multi-center study. Surg Endosc 31, 4315-4324 (2017)

6. Ginsburg, M., Zivin, S.P., Wroblewski, K., Doshi, T., Vasnani, R.J., Ha, T.G.V.: Comparison of Combination Therapies in the Management of Hepatocellular Carcinoma: Transarterial Chemoembolization with Radiofrequency Ablation versus Microwave Ablation. Journal of Vascular and Interventional Radiology 26, 330-341 (2015)
7. Andersen, I.R., Mortensen, F.V., Kirkegaard, J., Rasmussen, F., Nielsen, D.T., Kjaer, D.W.: Long-term survival following ablation of colorectal liver metastases. Journal of Surgery 6, 13-18 (2018)
8. Kopetz, S., Chang, G.J., Overman, M.J., Eng, C., Sargent, D.J., Larson, D.W., Grothey, A., Vauthey, J.N., Nagorney, D.M., McWilliams, R.R.: Improved Survival in Metastatic Colorectal Cancer Is Associated With Adoption of Hepatic Resection and Improved Chemotherapy. Journal of Clinical Oncology 27, 3677-3683 (2009)
9. Leung, U., Kuk, D., D'Angelica, M.I., Kingham, T.P., Allen, P.J., DeMatteo, R.P., Jarnagin, W.R., Fong, Y.: Long-term outcomes following microwave ablation for liver malignancies. British Journal of Surgery 102, 85-91 (2015)
10. Ludemann, L., Wlodarczyk, W., Nadobny, J., Weihrauch, M., Gellermann, J., Wust, P.: Non-invasive magnetic resonance thermography during regional hyperthermia. Int. J. Hyperthermia 26, 273-282 (2010)
11. Ebbini, E.S., Simon, C., Liu, D.: Real-Time Ultrasound Thermography and Thermometry. Ieee Signal Processing Magazine 35, 166-174 (2018)
12. Yarmolenko, P.S., Moon, E.J., Landon, C., Manzoor, A., Hochman, D.W., Viglianti, B.L., Dewhirst, M.W.: Thresholds for thermal damage to normal tissues: An update. Int. J. Hyperthermia 27, 320-343 (2011)
13. Clements, L.W., Collins, J.A., Weis, J.A., Simpson, A.L., Adams, L.B., Jarnagin, W.R., Miga, M.I.: Evaluation of model-based deformation correction in image-guided liver surgery via tracked intraoperative ultrasound. Journal of Medical Imaging 3, (2016)
14. Clements, L.W., Collins, J.A., Weis, J.A., Simpson, A.L., Kingham, T.P., Jarnagin, W.R., Miga, M.I.: Deformation correction for image guided liver surgery: An intraoperative fidelity assessment. Surgery 162, 537-547 (2017)
15. Heiselman, J.S., Clements, L.W., Collins, J.A., Weis, J.A., Simpson, A.L., Geevarghese, S.K., Kingham, T.P., Jarnagin, W.R., Miga, M.I.: Characterization and correction of intraoperative soft tissue deformation in image-guided laparoscopic liver surgery. Journal of Medical Imaging 5, (2018)
16. Boresi, A.P., Chong, K.P., Lee, J.D.: Elasticity in Engineering Mechanics. John Wiley & Sons, Inc., New York (2011)
17. COMSOL Inc., COMSOL Multiphysics Reference Manual. (2013)
18. Collins, J.A., Heiselman, J.S., Clements, L.W., Brown, D.B., Miga, M.I.: Multiphysics modeling towards enhanced guidance in hepatic microwave ablation: A preliminary framework. Journal of Medical Imaging (in review) (2019)
19. Marengo, A., Rosso, C., Bugianesi, E.: Liver Cancer: Connections with Obesity, Fatty Liver, and Cirrhosis. In: Caskey, C.T. (ed.) Annual Review of Medicine, Vol 67, vol. 67, pp. 103-117 (2016)